Proceedings of the NATO Advanced Research Workshop on Theoretical Immunology held in Paris, September 27- October 1, 1991

ISBN 3-540-54614-6 Springer-Verlag Berlin Heidelberg New York
ISBN 0-387-54614-6 Springer-Verlag New York Berlin Heidelberg

Library of Congress Cataloging-in-Publication Data
Theoretical and experimental insights into immunology / edited by Alan S. Perelson, Gérard Weisbuch.
(NATO ASI series. Series H, Cell biology ; vol. 66)
Includes bibliographical references and index.
ISBN 3-540-54614-6 (Berlin) ISBN 0-387-54614-6 (New York)
1. Experimental immunology–Congresses. 3. Immunology–Computer simulation–Congresses. I. Perelson, Alan S., 1947- II. Weisbuch, G. III. Series. QR180.3.T48 1992 616.07'9--dc20

Printed in Germany

Typesetting: Camera ready by author
31/3145 - 5 4 3 2 1 0 - Printed on acid-free paper

Growth and Recruitment in the Immune Network

Rob J. De Boer and Pauline Hogeweg
Bioinformatica
University of Utrecht
Padualaan 8
3584 CH Utrecht
The Netherlands

Alan S. Perelson
Theoretical Biology and Biophysics
Theoretical Division
Los Alamos National Laboratory
Los Alamos, NM 87545, USA

Abstract

The development of the immune repertoire during neonatal life involves a strong selection process among different clones. We investigate the hypothesis that repertoire selection is carried out during early life by the immune network. There are at least two processes in repertoire selection: clonal expansion and recruitment of clones by the bone marrow. Because both processes occur on time scales of the order of a few days, we argue that both have to be modeled. In a previous differential equation model (De Boer & Perelson, 1991), studied by numerical integration, both clonal expansion and recruitment were present but the rate of recruitment was kept low due to limitations in computational resources.

Here we present a new model based upon a two-dimensional shape space. The model is defined as an asynchronous cellular automaton (CA). In the CA model we vary (1) the rate of recruitment and (2) the specificity of the lymphocyte receptors. The networks attain an equilibrium in which the size of the repertoire remains fixed. However, the equilibrium repertoire size increases when the recruitment rate or the receptor specificity is increased. The number of functional idiotypic interactions per clone, i.e., the connectivity, is less dependent on either the receptor specificity or the recruitment rate. These observations confirm the results of our previous study. The CA model contributes to our understanding of pattern formation in immune network models because of its straightforward visualization. Using it we show that the randomness involved in lymphocyte recruitment may play a role in selecting the clones in the actual repertoire.

NATO ASI Series, Vol. H 66
Theoretical and Experimental Insights into Immunology
Edited by A. S. Perelson and G. Weisbuch

Introduction

Due to the massive production of novel lymphocyte clones in the bone marrow the composition of the immune network (Jerne, 1974) is variable. The B lymphocyte network is composed of a large number of clones, possibly as many as 10^6 to 10^8. Each clone is characterized by the variable (V) portion of its immunoglobulin receptor. B cell clones are produced in the bone marrow where reshuffling of gene segments leads to the generation of a large number of possible V regions. The diversity of receptor molecules created by gene reshuffling in the bone marrow suggests that any particular arrangement of gene segments and somatic mutations is likely to be unique. Thus, established clones are not expected to be resupplied by the bone marrow.

If stimulated properly, recirculating B cells expand in the periphery by cell division, giving rise to a clone of cells expressing the same receptor. The dynamics of recirculating B cell clones are governed by cell division and cell death. Because B cells have a life time of a few days, and because cell division typically takes less than one day, the characteristic time scale of the growth of an individual clone is on the order of days. In the adult mouse, it is estimated that the production in the bone marrow amounts to $2 - 5 \times 10^7$ B cells per day (Freitas *et al.*, 1986). This is sufficient for replacing the entire B cell population in just a few days. It thus seems that the time scale at which clones are replaced by bone marrow production and the time scale at which clones grow, are both on the order of days. In this respect, immune networks are very different from neural networks where neurons live for years but may switch from resting to firing on a time scale of milliseconds.

The importance of bone marrow recruitment as a means of generating novel clones was first stressed by Farmer *et al.* (1986; 1987) and later by Varela and co-workers (Varela *et al.*, 1988; Varela & Stewart, 1990; Stewart & Varela, 1989, 1990, 1991). In the original Varela papers recruitment was incorporated in a very rudimentary form. The bitstring models of Farmer *et al.* (1986,1987) incorporated more elaborate attempts to model recruitment but dealt with unrealistic dynamical equations. Two recent papers try to remedy the situation. In De Boer & Perelson (1991) we succeeded in combining clonal growth and recruitment in a bitstring model using a more realistic model. However, due to computational problems we were unable to study the model for realistic recruitment rates. Stewart & Varela (1991) modeled recruitment but ignored clonal growth.

The generation of novel clones by recruitment has been ignored in most mathematical models of the immune network (see De Boer, 1991; De Boer *et al.*, 1992d; and Perelson, 1989 for reviews). For reasons of simplicity, it is usually assumed that each clone has a continuous supply of cells from the bone marrow. This simplified view need not be incorrect however. First, genetically different receptors may form the same idiotype. Thus, one may view the populations of a network model as a collection of different clones having the same idiotype. Second, it is known that the B cells that appear first in ontogeny have receptors that are germ line encoded and are based upon a limited number

V_H gene families (Holmberg *et al.*, 1989). This reduces the diversity and increases the likelihood that established clones are recruited again by the bone marrow.

In this paper we take an intermediate position and assume that idiotypes (which may correspond to multiple clones) are recruited on a stochastic basis. We develop a stochastic cellular automaton model that allows us to combine clonal growth and recruitment on any time scale. By varying the recruitment rate P_R we study its impact on the model's behavior.

Bell-Shaped Activation Function

Most recent immune network models are based upon the bell-shaped interaction function proposed by De Boer (1988) or upon the two biphasic interaction functions proposed by Varela *et al.* (1988). The bell-shaped activation function $f(h)$ that we use takes the form,

$$f(h) = \frac{h}{\theta_1 + h} \frac{\theta_2}{\theta_2 + h} , \tag{1}$$

where $\theta_1 \ll \theta_2$. The first factor in $f(h)$ increases from 0 to 1, reaching its half-maximal value at $h = \theta_1$, the second factor decreases from 1 to 0, reaching its half-maximal value at $h = \theta_2$. For $\theta_2 \gg \theta_1$, the maximum is approximately one. This maximum is attained at $h = \sqrt{\theta_1 \theta_2}$. The "field" h measures the effective amount of anti-idiotype a clone interacts with, and depends on both the number of anti-idiotype clones and the strength of their interaction with the idiotype (see below). Plotted as a function of $\log h$, the graph of $f(h)$ is a bell-shaped curve. An important argument for the use of a log bell-shaped function is that receptor crosslinking is involved in B cell activation. For ligands that are bivalent the cross-linking curve is bell-shaped and symmetric around its maximum (Perelson & DeLisi, 1980; Perelson, 1984).

Clonal growth is typically described in terms of differential equations. The most realistic models require several differential equations for each idiotype describing the production of antibody, B cell maturation, antibody recirculation, and so on. However, all previous models are centered around a simple differential equation describing the growth of one clone of B cells, b,

$$db/dT = b[Pf(h) - d] , \tag{2}$$

where h is the field of the clone, $f(h)$ is defined by Eq. (1), P the maximum rate of proliferation, and d is the rate of cell death. The model is non-dimensionalized by scaling the time T to the rate at which B cells turn over:

$$db/dt = b[pf(h) - 1] , \tag{3}$$

where $t = Td$ and $p = P/d$. Because $0 \leq f(h) < 1$, B cells can grow at a maximal rate $p - 1$. Thus, in order to allow for net clonal expansion p must be greater than 1. Since maximally stimulated cells divide about once every 16 h, and cells live a few days (e.g., $d = 0.5$ d^{-1}), $p = 2$ is a typical non-dimensional rate of proliferation.

Shape Space

A powerful formalism for defining the field h of each clone is the shape space theory (Perelson & Oster, 1979; Segel & Perelson, 1988, 1989, 1990; De Boer *et al.*, 1992a). Interactions amongst the clones depend on complementarities between the immunoglobulin receptors characteristic of each clone. The degree of binding of two idiotypes, usually measured by their equilibrium binding constant or affinity, depends on the generalized shapes of the two receptor molecules involved (Perelson & Oster, 1979). Thus, we let each population be characterized by a generalized shape $\mathbf{x}$. (In a multidimensional shape space $\mathbf{x}$ is a vector.) To specify the field, h, one assumes cells of shape $\mathbf{x}$ are mainly stimulated by cells of complementary or near-complementary shape $\hat{\mathbf{x}}$ centered around $\mathbf{x} = -\mathbf{x}$. The affinity or the degree of interaction between shapes $\mathbf{x}$ and $\hat{\mathbf{x}}$ usually decreases according to a Gaussian function. The Gaussian function is based upon an exponential fall off,

$$g(\mathbf{x}, \hat{\mathbf{x}}) = \exp[-\frac{|\mathbf{x} + \hat{\mathbf{x}}|^2}{\sigma^2}] \ , \tag{4}$$

where the standard deviation, σ, defines the rate at which the affinity falls off with the distance to the perfect match $\mathbf{x} = -\mathbf{x}$, see Segel & Perelson (1988).

An Asynchronous Cellular Automaton Model

A CA is a lattice of finite state machines. Each machine has a next state function that usually takes the local neighborhood of the machine on the lattice as input. In a previous paper (De Boer *et al.*, 1992a) we derived a discrete lattice mapping from a network model formulated in terms of partial differential equations (PDEs). This has the advantage that the conditions for stability of equilibrium states which were derived for the PDE system, provide an intuition for understanding the behavior of the lattice model. Here we follow our earlier simplifications and derive a CA model from the differential equation model defined by Eqs. (1-3).

First, we change to logarithmic variables $B = \ln b$. Second, we approximate $f(h)$ by the window automaton $w(h)$, originally proposed by Neumann and Weisbuch (1991), and defined as

$$w(h) = \begin{cases} 1 & \text{if } \exp(\theta_1) \leq h < \exp(\theta_2) \\ 0 & \text{otherwise} \end{cases} \ ; \tag{5}$$

Inserting this approximation into Eq. (3), and changing to logarithmic variables, we obtain

$$dB/dt = pw(h) - 1 \ . \tag{6}$$

As a consequence dB/dt in Eq. (6) increases at a rate $p-1$ when $w(h) = 1$, and decreases at a rate -1 when $w(h) = 0$. Choosing $p = 2$, dB/dt can be only 1 or -1. Third, we discretize time and take integer variables for B to simplify Eq. (6) into the mapping

$$B(t+1) = B(t) + 2w(h) - 1 \ . \tag{7}$$

Fourth, in order to have a *finite* state machine we impose lower and upper limits on $B(t)$. A natural lower limit is $b(\mathbf{x}) = 1$, i.e., $B(\mathbf{x}) = 0$, which is thus the equivalent of a site with a single B cell. In the CA with recruitment, sites can also be empty, i.e., contain no B cells. We denote empty sites with $B(\mathbf{x}) = -1$. Empty sites never contribute to fields. As an upper limit we chose $B(t) \leq \theta_3$, which corresponds to a population maximum of $\exp[\theta_3]$ B cells. A population maximum seems reasonable because B cells are not capable of infinite proliferation and typically go through a maximum of about eight divisions (Klinman *et al.*, 1984). This gives us the next state function for the clonal growth

$$B(t+1) = \min[\theta_3, \max[-1, B(t) + 2w(h) - 1]] \,, \tag{8}$$

by which clones sizes are limited between $-1 \leq B(t) \leq \theta_3$.

In one simplification of the CA we replace the recruitment by a continuous source of cells. This is implemented by changing the lower limit for the population at a single latice site to one B cell:

$$B(t+1) = \min[\theta_3, \max[0, B(t) + 2w(h) - 1]] \,. \tag{9}$$

Finally, in combination with the next state function Eq. (8), which models clonal growth, we need a next state function for stochastic recruitment. If a recruitment event occurs, then the bone marrow adds the equivalent of one B cell, i.e., $B = 0$, to sites that are empty. Thus,

$$B(t+1) = \begin{cases} 0 & \text{if } B(t) = -1 \,; \\ B(t) & \text{if } B(t) \geq 0 \,. \end{cases} \tag{10}$$

We implement the next state functions as a 2D cellular automaton using an integer 2D shape vector $\mathbf{x}$ that is bounded between $[-N, -N] \leq \mathbf{x} \leq [N, N]$. We thus have a CA defined on a lattice of $(2N+1)^2$ sites. The self-complementary shape $[0, 0]$ is located in the center of the lattice. Because we can scale distances using the standard deviation σ, we can use $\mathbf{x}$ for both shape and for the latice site index in the automaton.

Neighborhoods. The affinity falls off with the distance to the perfect match according to the Gaussian fall-off $g(\mathbf{x}, \hat{\mathbf{x}})$ defined in Eq. (4). Thus, the contribution to the field $h(\mathbf{x})$ made by a single clone $b(\hat{\mathbf{x}}) = \exp[B(\hat{\mathbf{x}})]$ is given by

$$h(\mathbf{x}) = b(\hat{\mathbf{x}}) g(\mathbf{x}, \hat{\mathbf{x}}) \quad \Leftrightarrow \quad h(\mathbf{x}) = \exp[B(\hat{\mathbf{x}}) - G(\mathbf{x}, \hat{\mathbf{x}})] \,, \tag{11}$$

where

$$G(\mathbf{x}, \hat{\mathbf{x}}) = \frac{|\, \mathbf{x} + \hat{\mathbf{x}} \,|^2}{\sigma^2} \,. \tag{12}$$

The field $h(\mathbf{x})$ and the function $G(\mathbf{x}, \hat{\mathbf{x}})$ are again integer variables. Because $h(\mathbf{x})$ is integer, all contributions for which $\exp[B(\hat{\mathbf{x}}) - G(\mathbf{x}, \hat{\mathbf{x}})] < 1$ are ignored by integer truncation.

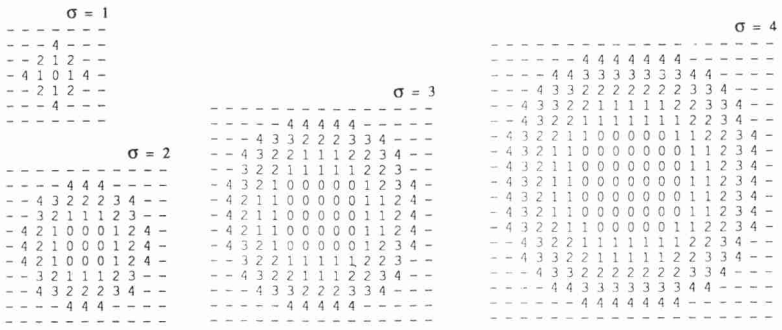

Figure 1. The CA's neighborhood weighting around the perfect match $\mathbf{x} = -\mathbf{x}$ as it is defined by the Gaussian function $G(\mathbf{x}, \hat{\mathbf{x}})$. The Gaussian is truncated at $\Delta = 4$: the sites indicated by a $-$ are ignored. Four neighborhoods correspond to $\sigma = 1, 2, 3, 4$ are shown. For $\sigma = 1, \ldots, 5$, the total number of sites in the neighborhood is 13, 61, 137, 241, and 385, respectively.

In immunological terms this means that the affinity of the idiotypic interaction decreases as a function of $G(\mathbf{x}, \hat{\mathbf{x}})$ in the CA. Because low affinities do not seem to lead to B cell stimulation (Fish *et al.*, 1989; Riley & Klinman, 1986; Klinman, 1972) we have implemented an affinity cut-off. In the CA formalism an affinity cut-off is naturally defined by the size of the neighborhood (see also De Boer *et al.*, 1992a). Thus, we let Δ be the value of $G(\mathbf{x}, \hat{\mathbf{x}})$ at the maximum interaction distance in shape space and ignore all larger values of $G(\mathbf{x}, \hat{\mathbf{x}})$. In Fig. 1 we show examples of our Gaussian function for $\Delta = 4$ and $\sigma = 1, 2, 3, 4$. The radius r of the neighborhood of the CA can be obtained from Fig. 1. For $\sigma = 1, 2, 3, 4, 5$, $r = 2, 4, 6, 8, 11$ respectively.

Finally, for the calculation of the field we will only consider populations for which $B(\hat{\mathbf{x}}) > 0$. We thus ignore empty lattice sites ($B = -1$) and sites that contain a single B cell ($B = 0$). Thus contributions to the field are only made by populations that have divided and are in a non-resting state. The reason for doing this is that a clone should not be stimulated to grow by a field totally comprised of virgin clones, i.e., clones that just appeared from the bone marrow. Typically, interactions between clones are not direct B cell–B cell interactions but are mediated by secreted antibodies carrying the idiotype of the B cell. Since resting clones do not secrete antibody, the exclusion of resting clones from the field seems desireable. Under this assumption, for any shape $\mathbf{x}$ the total field $h(\mathbf{x})$ correponds to

$$h(\mathbf{x}) = \sum_{\hat{\mathbf{x}} \in C(-\mathbf{x})} \exp[B(\hat{\mathbf{x}}) - G(\mathbf{x}, \hat{\mathbf{x}})] \ , \quad \forall \ B(\hat{\mathbf{x}}) > 0 \ , \tag{13}$$

where $C(-\mathbf{x})$ is the circle centered at $-\mathbf{x}$ with radius r. We assume fixed boundaries, i.e., shapes outside the shape space $[-N, -N] \leq \hat{\mathbf{x}} \leq [N, N]$ are fixed at concentration -1.

Scheduling. The sites of a CA can be updated in parallel, i.e. synchronously, or randomly, i.e. asynchronously. Most of our results are based upon asynchronous updating. We choose this method updating so that we can independently vary clonal growth and recruitment events. Thus, for each update we randomly choose one of the two next state functions Eqs. (8) or (10). The parameter P_R defines the probability with which the recruitment event is chosen. Because there are only two types of events, clonal growth is chosen with probability $1 - P_R$. The selection of the site to be updated is also random. We will only present results for which the site selection is based upon a uniform distribution in the interval $[-N, N] \leq \mathbf{x} \leq [N, N]$. Thus, the basic iteration cycle is (1) select a site to be update, (2) select a transition function, and (3) perform the update.

Parameters. We have previously studied models based upon Eq. (3) for $\theta_1 = 100$ and $\theta_2 = 10^4$. In the CA we convert θ and h values to logarthmic variables. Thus, we round these values of θ to $\theta_1 = 5$ because $\exp[5] \approx 148$ and $\theta_2 = 10$ because $\exp[10] \approx 2.2 \times 10^4$. In order to reduce the effect of the maximum population size we set $\theta_3 \gg \theta_2$. Choosing $\theta_3 = 15$, each B cell population can maximimally grow to $\exp[15] \approx 3 \times 10^6$ cells. This is probably a high estimate because B cell proliferation is typically limited to eight divisions or so (Klinman *et al.*, 1984). The affinity cut-off is set to $\Delta = \theta_3 - \theta_2 - 1$. By Eq. (11), the field contribution of a clone at maximum size, i.e., $B = \theta_3$, must be at least $h = \theta_3 - \Delta = \theta_2 + 1$. Thus, a clone at maximum size can only evoke a suppressive field. This seems reasonable because we do not want the network to sustain clones at a probably unreasonable maximum size. If equilibrium populations $B(\mathbf{x}) = \theta_3$ are allowed to have stimulatory effects on other populations, i.e., if $\Delta > \theta_3 - \theta_2$, the behavior of the CA becomes reminiscent of the model of Stewart and Varela (1991) and De Boer and Van der Laan (1992). The system forms stable lines of clones of maximum size. The distance between the lines is such that they reciprocally activate each other (not shown).

We choose $N = 50$, i.e., we work on a 101×101 lattice. This corresponds to a potential repertoire of $101^2 \approx 10^4$ clones. The results show that the CA never fills all sites of the lattice. The sites filled with B cell populations correspond to the actual repertoire. Choosing $\sigma = 3$ as the standard value for the size of the neighborhood each clone can have a maximum of 25 high affinity interactions, see Fig. 1. The total number of clones in the $\sigma = 3$ neighborhood is 137 idiotypes, which is roughly 1% of the total shape space. As a default we choose equal time-scales for proliferation and recruitment, i.e., we set $P_R = 0.5$.

Computation. The CA was implemented in the C programming language. The code is available electronically from *deboer@cc.ruu.nl.* Simulations were performed on a Silicon Graphics Personal Iris. Depending on the size of the neighborhood this took several hours. In principle the code is efficient because the various exponents required for summing the field, and for the Gaussian fall-off Eq. (12), can be stored as integer arrays that need only be computed once. The remainder of the computation boils down to stepping through the 2D shape space array, and performing the integer subtraction and addition implied by Eq. (13). Random numbers for site selection and event selection

were computed with the RAN3 routine described in "Numerical Recipes" (Press, *et al.*, 1988).

Since clones expand and decrease one order of magnitude on a time scale of days, we base the time steps of our model on the clonal growth function. Time is increased one unit after $(2N+1)^2$ evaluations of the next state functions Eq. (8) or (9). This means that, on average, during each time step all clones in the CA will have updated their state. Thus, the time clock clicks independent of the recruitment. Typically the CA was studied for 500 time steps.

Previous Models

The two recent models of the recruitment of the immune system are very different from each other. In the work of De Boer and Perelson (1991) the generalized shape $\mathbf{x}$ takes the form of a bit-string, i.e., a point in a high-dimensional hypercube. Clonal growth is modeled by means of a system of differential equations based on Eq. (2). Recruitment is implemented by interrupting the numerical integration, and changing number of differential equations that model clonal growth as clones are added or deleted. The recruitment is based upon the addition of B cell populations created by an artificial bone marrow, and the deletion of populations that have grown smaller than one single cell. The main problem with this approach is that computational resources limit the number of populations that the artificial bone marrow can add to the system. Thus the system could not be studied for realistic recruitment rates.

In the work of Stewart and Varela (1991) the generalized shape $\mathbf{x}$ takes the form of a point in a 2D shape space. Clones in the shape space are either present or absent, and clonal growth is ignored. The equivalent of the bell-shaped interaction function of the clonal growth process is put directly into the recruitment process. Clones are maintained in the network if the number of interaction partners, weighted by the respective distances in shape space according to Eq. (4), falls within a window set by two parameters θ_1 and θ_2. Clones can only be added to the network if their field falls within the window. Once a clone is added to the network the fields of all established clones are checked. If a clone's field falls outside the window that clone is deleted. The check then has to be repeated because the fields have changed again. This iteration halts when all clones have a field inside the window. In the worst case all clones are deleted. Note that the algorithm depends on the order by which the clones are scanned, and hence, that it may collapse, i.e., delete all clones, in situations where better solutions are possible. However, because of the similar time scales of clonal growth and of the recruitment, the main problem with this work is that clonal growth is ignored. Since the size of a clone is important in determining the field that it generates, this model ignores a very important aspect of network dynamics.

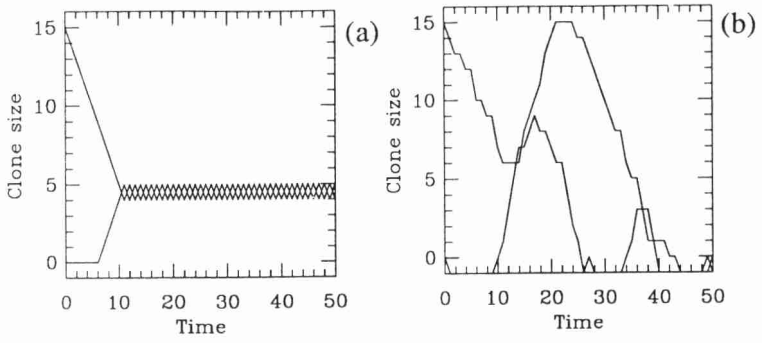

Figure 2. Time plots of a two clone system $h_1 = \exp[B_2] + \exp[A]$ and $h_2 = \exp[B_1]$. Parameters: $\theta_1 = 5, \theta_2 = 10, \theta_3 = 15$, and $P_R = 0.5$. (a) Parallel updating without recruitment, i.e., a model based upon Eq. (9). Initial conditions: $B_1(0) = 15$, $B_2(0) = 0$. (b) Asynchronous updating with stochastic recruitment, i.e., a model based upon Eqs. (8 & 10). Initial conditions: $B_1(0) = 15$, $B_2(0) = 0$.

Results

In this paper we use an asynchronous CA model of the immune network. With this model it is possible to combine clonal growth and recruitment at the correct time scales. Our principle point of interested is whether the results of the CA model differ from the results of our previous bit-string model (De Boer & Perelson, 1991). The main parameters that we varied in the bit-string model were the specificity of the receptors and the rate of production of new clones by the bone marrow. The latter parameter corresponds to the recruitment in the CA. In the bit-string model the rate of recruitment is expressed as the daily production of novel bit-strings by the artificial bone marrow. The specificity of the receptors was determined by the rules by which two bit-strings were matched. This was expressed as the "reactivity" of the receptors or $P(match)$, i.e., the fraction of other receptors each receptor is expected to bind. The reactivity was varied between binding probabilities of 0.005 and 0.205. Henceforth, we refer to our previous model as the bit-string model.

Two Interacting Clones

The basic dynamics of the next state functions Eqs. (8–10) can be studied by simulating two interacting clones instead of simulating the full CA. Thus, let $B_i(t)$, for $i = 1, 2$, be defined by Eqs. (8–10), and let the field of clone B_1 be $h_1 = \exp[B_2]$ and the field

of clone B_2 be $h_2 = \exp[B_1]$. (In the orginal formulation of differential equations like Eq. (2) such two clone systems may give rise to stable equilibria, limit cycle oscillations, or chaos, depending upon parameter values, see De Boer & Hogeweg, 1989a,b; De Boer *et al.*, 1990, 1992b,c).

The simplest case is a system with parallel updating of B_1 and B_2 according to function Eq. (9). We show, in Fig. 2a, a simulation for the initial condition $B_1(0) = \theta_3$ and $B_2(0) = 0$, for the parameters $\theta_1 = 5$, $\theta_2 = 10$, $\theta_3 = 15$. Because $h_1 = 0$, B_1 decreases due to a lack of stimulation. B_2 cannot grow due to suppression, i.e., $h_2 > \theta_2$. B_2 starts to grow after $\theta_3 - \theta_2$ time steps, when B_1 has decreased to $B_1 = \theta_2$. B_1 stops decreasing after another θ_1 time steps, when B_2 has increased to $B_2 = \theta_1$. The two clones attain an attractor around θ_1 alternating between giving stimulation while decreasing due to a lack of stimulation, and not giving stimulation while increasing, see Fig. 2a. In a system with parallel updating, such a stable attractor around θ_1 is always present. The other attractors are the oscillator $B_1 = B_2 = \theta_2 \rightarrow B_1 = B_2 = \theta_2 - 1 \rightarrow B_1 = B_2 = \theta_2, \ldots$, and the equilibrium$B_1 = B_2 = 0$. It depends on the initial conditions which of the three attractors is attained.

The same system with asynchronous updating, i.e., one based upon Eqs. (8 & 10), behaves differently. See Fig. 2b for an example with $P_R = 0.5$. The attractor around θ_1 is no longer stable because by random chance both clones may equal θ_1. They then stimulate each other reciprocally until one of them equals θ_2. Typical behavior of the asynchronous automaton is large variations in the population densities, see Fig. 2b. In this respect the behavior resembles the oscillatory/chaotic behavior of the continuous model (De Boer *et al.*, 1990, 1992c,d).

Cellular Automaton

We study the immune network as it develops during early ontogeny. In vivo this corresponds to a situation in which most self-antigens are present and B cells are absent. Network interactions could develop when autoreactive B cells are stimulated by self-antigens and subsequently start to activate anti-idiotypic B cells. Another possibility is that anti-idiotypic B cells are activated by so-called maternal antibodies which the developing system obtains from the mother. In our previous work we started the network with maternal antibodies (De Boer & Perelson, 1991). Here we start similarly by setting 1% of the shapes to the stimulatory concentration $B(\mathbf{x}) = (\theta_1 + \theta_2)/2$. These populations represent the maternal antibodies. All other sites are assumed to be empty, i.e., $B(\mathbf{x}) = -1$.

In Figs. 3 and 4 we show an example of the model's behavior. In Figs. 3a and 3b we show a snapshot of the CA after 500 time steps. The 2D distribution of the clone size $B(\mathbf{x})$ is shown in Fig. 3a and the log field size $\ln[h(\mathbf{x})]$ in Fig. 3b. The size of the population is indicated by gray-scales, where black means large and white means small. The 2D distribution of clones typically takes the form of lines and circles. The 2D

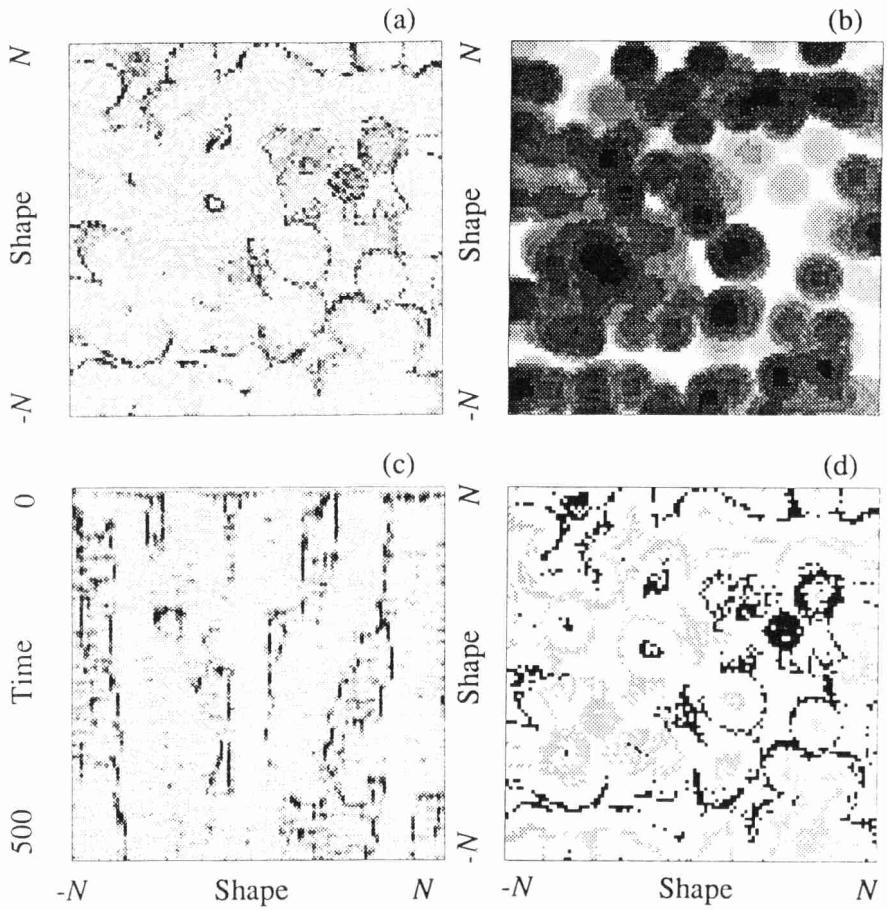

Figure 3. Shape space usage in an asynchronous CA. Parameters: $\sigma = 3, \theta_1 = 5, \theta_2 = 10, \theta_3 = 15, \Delta = 4$, and $P_R = 0.5$. (a) The 2D clone size distribution attained after 500 time steps. The gray-scales vary between white for $B(\mathbf{x}) = -1$ and black for $B(\mathbf{x}) = \theta_3$. (b) The log fields, i.e., $\ln[h(\mathbf{x})]$, corresponding to panel (a). The gray-scales vary between white for $\ln[h(\mathbf{x})] = 0$ and black for $\ln[h(\mathbf{x})] = 17$. (c) A space time plot for all clones along one diagonal of the shape space, i.e., $\{\forall\, B(x,x) \mid x = -N, \ldots, x = N\}$. (d) The 2D clone size distribution shown in panel (a). For each each point in shape space $\mathbf{x}$ the color is white if $B(\mathbf{x}) < \theta_1$ and $B(-\mathbf{x}) < \theta_1$, otherwise the color is black if $B(\mathbf{x}) > B(-\mathbf{x})$ and gray if $B(\mathbf{x}) < B(-\mathbf{x})$. Thus the black image corresponds to the real distribution of large clones. The gray pattern is the mirror image of the black pattern.

distribution of the fields typically takes the form of circular areas with the maximum field strength in the middle. This corresponds to a field landscape of hills and valleys. The comparison of the two distributions reveals that large clones are typically located at intermediate field strengths. This means that the clones live at the contour lines of intermediate height of the field landscape. The reason for this is clear: the window automaton $w(h)$ specifies that clones can only expand at intermediate field strengths. A more interesting observation is that the lines along which clones organize themselves are much longer than the size of the neighborhood of the automaton (i.e., a circle with radius $r = 6$). Thus the pattern that is attained by the self-organization has a much larger scale than the local rules of the automaton have.

In Fig. 3c we show a space-time diagram of the CA by sampling clone sizes along one diagonal of the shape space from $B(-N, -N)$ to $B(N, N)$. Thus, the self-complementary shape $B(0, 0)$ is located in the middle of the space axis. Time runs along the vertical axis from 0 to 500. The figure shows that the 2D distributions fail to attain a steady state but change and move about in shape space. The vertical dark lines in the figure correspond to clones that temporarily attain a stationary state and remain large for some time. The diagonal lines correspond to travelling waves. If one views these results in the form of movies of consecutive 2D distributions, travelling waves are a striking phenomenon. Fig. 3c shows that although the 2D distributions never attains a steady state the patterns change on a time-scale that is much slower than the time-scale of recruitment and clonal growth. The travelling waves and the patterns shown in Fig. 3a are reminiscent of the self-organization of excitable media and reaction-diffussion systems (cf. Murray, 1989). This type of behavior was also seen in the bitstring model of Farmer *et al.* (1986) as discussed by Perelson (1988).

To visualize which clones interact we project the mirror image of large clones onto the opposite part of the shape space. In Fig. 3d, we color all clones $\mathbf{x}$ that are larger than θ_1 black, and project their mirror image at $-\mathbf{x}$ in gray. The white spots correpond to sites $\mathbf{x}$ for which $B(\mathbf{x}) \leq \theta_1$ and $B(-\mathbf{x}) \leq \theta_1$. Thus, the distribution of black spots corresponds to large clones, and is identical to the distribution of dark-gray spots in Fig. 3a. The distribution of the gray spots is the mirror image of the black spots reflected about $[0, 0]$. The figure shows how the circles of clones enclose smaller circles of complementary clones, and how lines of clones are aligned with lines of complementary clones. The distance between the gray and the black patterns reflects the distance at which large clones evoke a stimulatory field. In Fig. 3a or 3d the self-complementary clone $[0, 0]$ does not seem to behave very different than any other clone.

Sampling global properties. In the bit-string model we showed that both the number of clones in the network and the connectivity of the network attains a maximum value during the early life of the network. Following this early peak the number of clones and the connectivity approach a much lower equilibrium. These observations correspond to experimental observations that show that the network connectivity is large during early life (Holmberg *et al.*, 1989). The notion of an equilibrium size of the immune network has also been suggested by experimentalists, see the discussion in De Boer & Perelson (1991). Here we study similar global properties of the CA networks. We sampled the

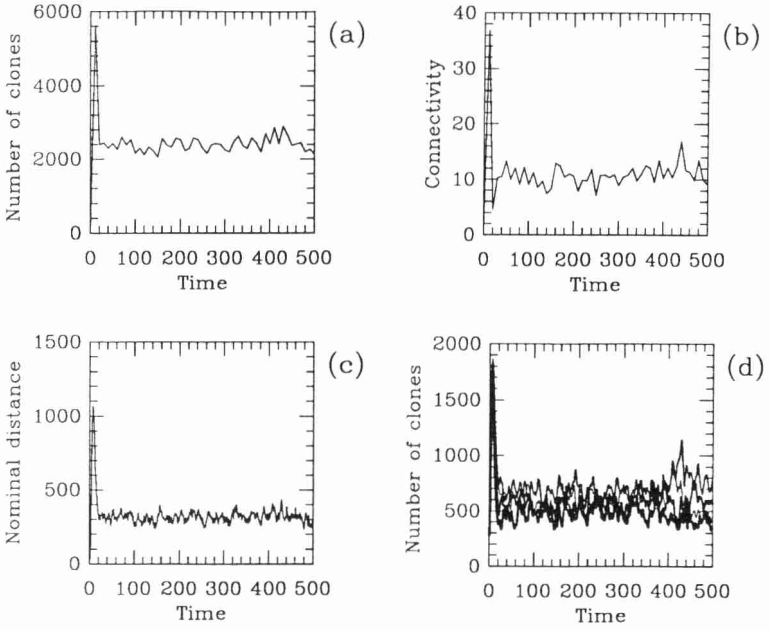

Figure 4. Global properties of an asynchronous CA. Parameters: $\sigma = 3, \theta_1 = 5, \theta_2 = 10, \theta_3 = 15, \Delta = 4$, and $P_R = 0.5$. (a) number of active clones. (b) actual connectivity. (c) nominal distance. (d) number of populations per quadrant.

number of active clones and the functional connectivity of the clones in the network. An active clone is a clone that is present and has divided, i.e., we count the number of non-zero clones. The functional connectivity is the number of active interaction partners of an active clone, i.e., we count the average number of non-zero clones in the neighborhood of each non-zero cell. Both properties are sampled every ten time steps.

For the example network of Fig. 3 we show time plots of the number of clones and the connectivity are shown in Figs. 4a and 4b. The results are very similar to the results of the bit-string model. Both the size of the network, i.e., the number of clones, and the connectivity go through an early peak, and then approach equilibrium levels. During the last 100 days of the simulation the average network size is 2466 clones with an average connectivity of 12 functional connections. Because the potential repertoire corresponds to 10^4 clones it appears that by repertoire selection 25% of the possible clones participate in the immune network.

Two other novel properties are shown in Figs. 4c and 4d. The rate at which the 2D distributions shown in Fig. 3 change is measured by the "nominal distance" between the patterns. We classify clone sizes into three categories: $B(\mathbf{x}) < \theta_1$, $\theta_1 \leq B(\mathbf{x}) < \theta_2$, and

$B(\mathbf{x}) \geq \theta_2$, and increase the nominal distance between two time steps one unit for each clone that switches to another category. A time plot of the nominal distance is shown in Fig. 4c. Following an early peak, the rate at which the patterns change approaches an equilibrium. Apparently, the actual repertoire is dynamic and continues to change. After a 1000 time steps the nominal distance is still very similar to the one shown in Fig. 4c (not shown). Finally, we counted the number of active clones in each of the four quadrants of the shape space. Time plots are shown in Fig. 4d. The averages during the last 100 time steps are 825, 570, 416, and 570, respectively. In order to test whether this deviates from a random distribution we calculated that $\chi^2 = 145$ for this distribution. With three degrees of freedom, $p < 10^{-4}$, so this is a very significant deviation from a random distribution.

Pattern Formation

The two main parameters that we varied in the bit-string model were the reactivity of the receptors (i.e., the bit-string matching) and the productivity of the bone marrow. In order to study the distribution of clones in the shape space of the bit-string model we computed the Hamming distances between all of the pairs of bit-strings in the network. If the coverage of shape-space is random, the distribution of Hamming distances is expected to be binomial. We showed that the bit-strings tended to be similar to each other, i.e., the Hamming distances were smaller than expected. The deviation increased with the rate of recruitment. We argued that these deviations were due to the formation of clusters of clones with similar bit-strings sharing the same stimulatory field. In the CA the reactivity and the productivity parameters correspond to the size of the neighborhood σ and the probability of recruitment P_R respectively. The effect of these parameters on pattern formation in shape space is studied in Figs. 5 and 6.

The 2D distributions shown in Fig. 5 reveal that the scale of the pattern scales with σ. First, the distance between the black and the gray stripes increases with σ. The explanation is that for large neighnorhoods clones have to be located far from each other to reduce the field strength. Second, the patterns become more global if σ increases. One striking "global" phenomenon which we observed repeatedly (Fig. 5c and 5d) are the long stripes that span the entire shape space. Such lines change position but seem to be anchored around shape $[0, 0]$. For large values of σ (Fig. 5d) the line forms the boundary between a density populated part of shape space and an empty part of shape space. Another global pattern that appears for large values of σ is that large regions in shape space tend to be either black or gray. Thus it seems that the usage of shape space changes from fine grained patterns to large scale clusters as σ increases.

In Fig. 6 we show the 2D distributions of large clones for $P_R = 0.1, 0.2, 0.4$, and 0.8. First, the figure shows that increasing P_R increases the thickness of the lines and the density of populated regions. Thus, areas in which the field is stimulatory are more densily populated. Because this increases the field strength, this implies that the distance between stripes has to increase. (This effect is so small that it is hardly visible.)

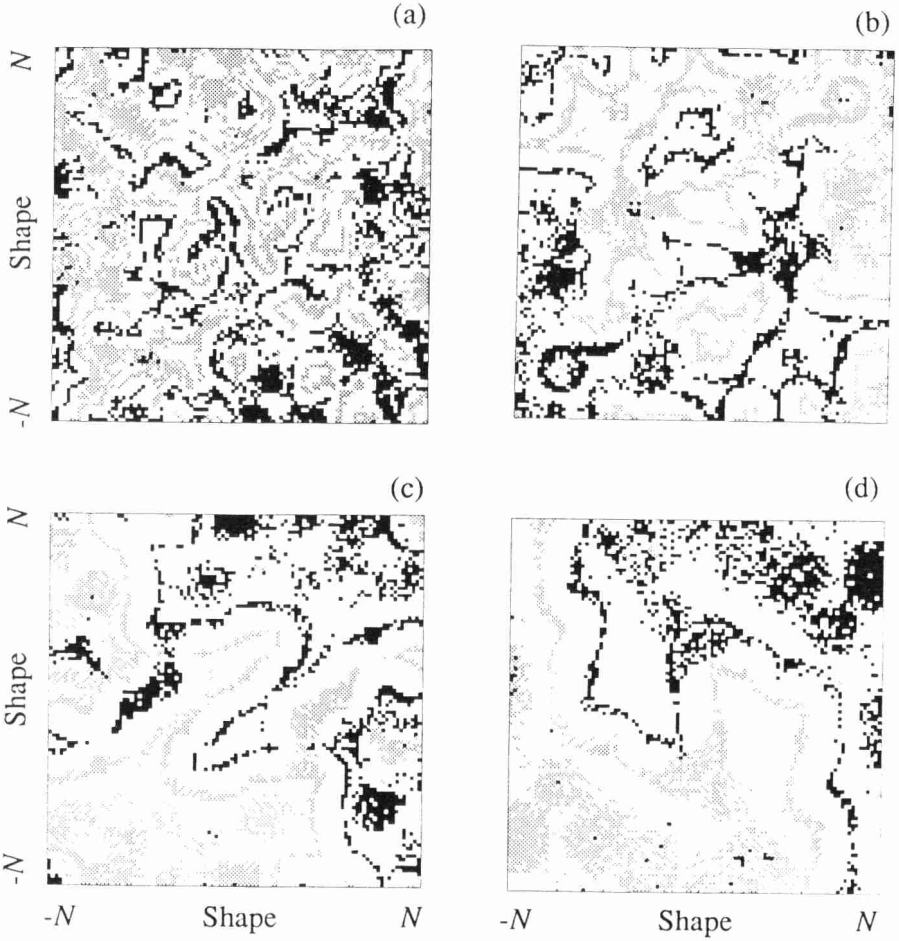

Figure 5. Shape space usage as a function of σ, the neighborhood size. Parameters: $\theta_1 = 5, \theta_2 = 10, \theta_3 = 15, \Delta = 4$, and $P_R = 0.5$. The gray-scales vary between white for $B(\mathbf{x}) = -1$ and black for $B(\mathbf{x}) = \theta_3$. (a) $\sigma = 2$. (b) $\sigma = 3$. (c) $\sigma = 4$. (d) $\sigma = 5$.

A densily populated area in shape-space means that idiotypes tend to be similar. This confirms the results of the bit-string model. The reason these patterns become more pronounced as P_R increases is that P_R determines the rate at which clones can invade areas with stimulatory fields. Second, on a larger scale, the figure shows that increasing the recruitment rate causes the repertoire selection to become more global. In Fig. 6a black and gray lines are distributed all over shape space. In Fig. 6d most clones are

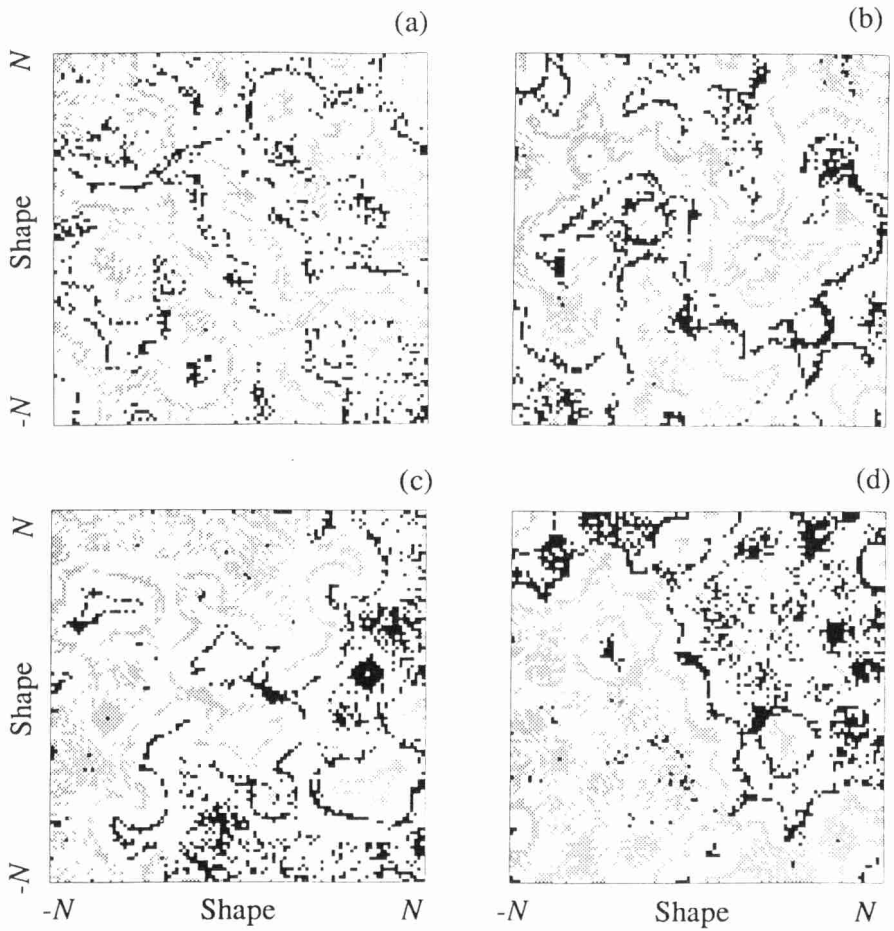

Figure 6. Shape space usage as a function of P_R, the rate of recruitment. Parameters: $\sigma = 3, \theta_1 = 5, \theta_2 = 10, \theta_3 = 15, \Delta = 4$. The gray-scales vary between white for $B(\mathbf{x}) = -1$ and black for $B(\mathbf{x}) = \theta_3$. (a) $P_R = 0.1$. (b) $P_R = 0.2$. (c) $P_R = 0.4$. (d) $P_R = 0.8$.

located in the upper right triangle of shape space. This is similar to what we observed for σ in Fig. 5.

As in Fig. 4d, we counted the number of active clones in each of the four quadrants. The χ^2 of the average distributions is plotted in Fig. 7a,b. This confirms the suggestion made above that the randomness of shape space usage decreases when σ or P_R increase. In Fig. 7c,d we plot the average nominal distance over the last 100 days of two simulations.

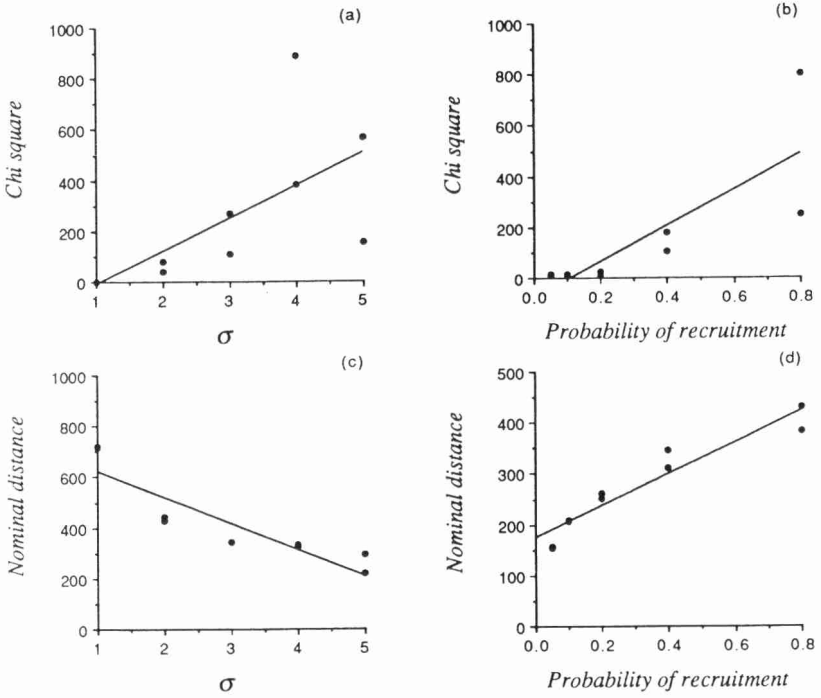

Figure 7. The scale and the rate of change of the shape space patterns. (a) χ^2 as a function of σ. (b) χ^2 as a function of P_R. (c) nominal distance as a function of σ. (d) nominal distance as a function of P_R.

When σ increases the rate of change of the patterns decerases. When P_R increases the rate of change of the patterns increases.

Pattern scale. We conclude that the scale of patterns increase with recruitment in both the bit-string model and in the asynchronous CA. The present results contribute to the understanding of these bit-string results because we now see how an increase in the recruitment decreases the randomness of the selected repertoire. This appears due to two effects. First, stimulatory areas are more rapidly invaded. This gives rise to a cluster of similar shapes. Second, the randomness involved with recruitment may play a role. Because novel clones are supplied at random sites and at random times, the rate of recruitment determines the degree of randomness in these systems. The fact that an increase in the randomness may increase the scale of the ordered regions in a CA has been described for voting rules. In voting rule systems frustration due to annealing (Vichnia, 1986), and/or simple random noise, create larger domains and a larger scale

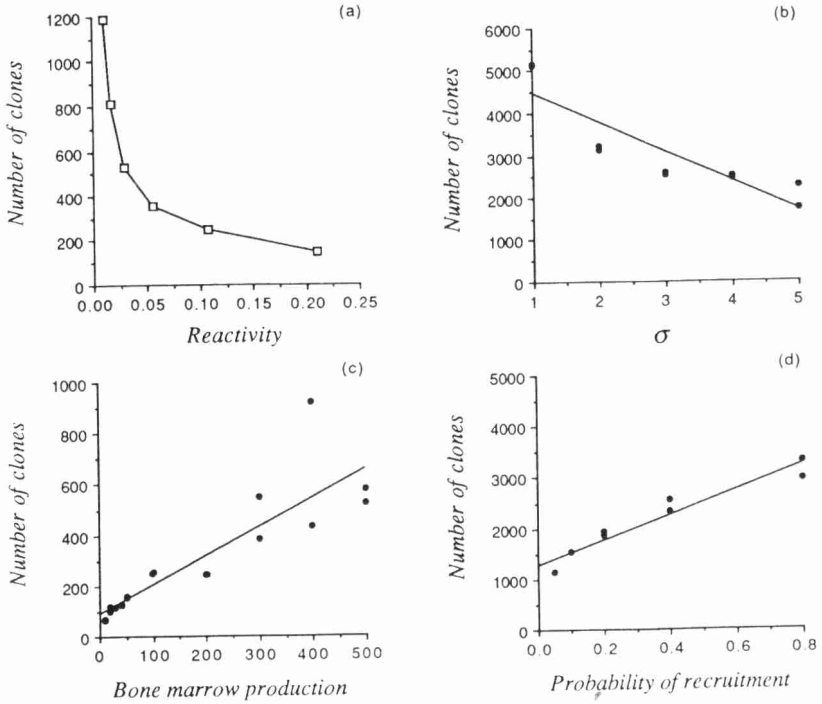

Figure 8. The number of clones in the repertoire. The network size as a function of reactivity in the bit-string model (a), and as a function of reactivity (i.e., σ) in the CA (b). The network size as a function of recruitment in the bit-string model (c) and in the CA (d).

of order (Toffoli & Margolus, 1987). Despite the fact that our transition rules Eqs. (8-10) are not voting rules, the randomness, which keeps boudaries fluid and which allows separate domains to merge, seems to have a similar effect in our immune network.

Size

One of the main question that we addressed in the bit-string model was the number of clones in the repertoire. Since there is no explicit regulation of the number of clones in the model the size of the network was an emergent property which turned out to vary around an equilibrium value. In Fig. 8 we show how the number of clones in the bit-string model varied as a function of the reactivity (Fig. 8a) and the productivity (Fig. 8c).

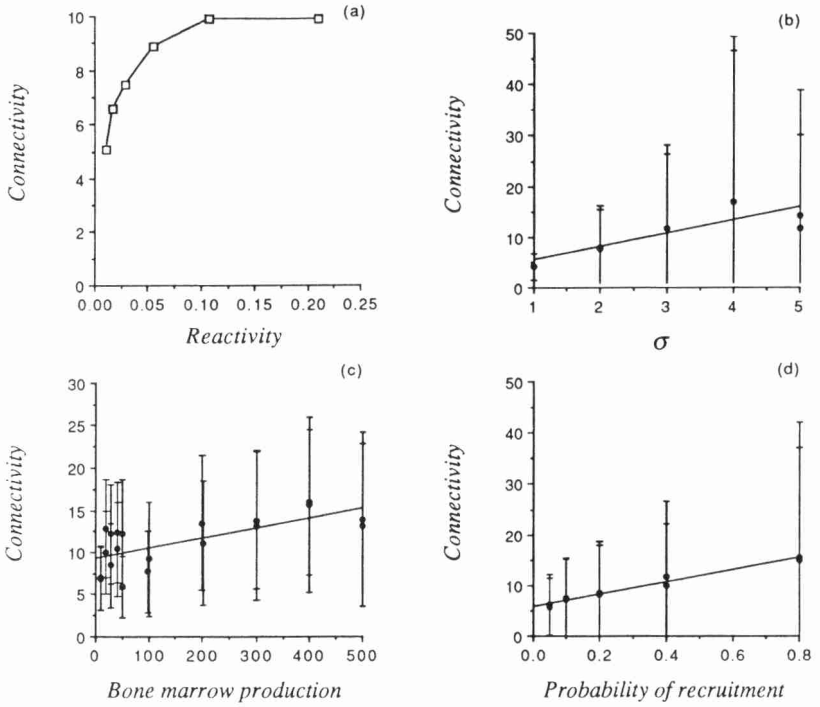

Figure 9. The actual connectivity of the repertoire. The network connectivity as a function of reactivity in the bit-string model (a), and as a function of reactivity (i.e., σ) in the CA (b). The network connectivity as a function of recruitment in the bit-string model (c) and in the CA (d). The error bars indicate the average standard deviation of ten samples.

In Figs. 8b and 8d we show that very similar results are obtained in the CA. Thus, increasing σ (i.e., the reactivity) decreases number of active populations. (Note that graphs in Fig. 8a and 8b would look more similar if the data in Fig. 8b were plotted as a function of the variance σ^2 instead of the standard deviation σ). In Fig. 8b the number of clones in the actual repertoire decreases from 5000 for $\sigma = 1$ to 2000 for $\sigma = 5$. Thus the selection for participation in the actual repertoire becomes stronger if σ or the reactivity increases. Conversely, the number of clones in the actual repertoire increases linearly as a function of the bone marrow production rate and of P_R. Thus, the shape space becomes more densily covered when the rate of recruitment increases. This can be explained by the formation of dense clusters of similar shapes.

Connectivity

Another emergent property of the bit-string model was the connectivity among the clone in the network, which like the network size varied around an equilibrium value. Connectivity was defined as the average number of network connections per clone. The results shown in Fig. 9a and 9c show that the connectivity of the network increases with reactivity and with bone marrow production rate. However, the increase in the connectivity is small compared to range over which the parameters are changed. Thus, we concluded that the connectivity is mainly regulated by selection in the network and is hardly dependent on the reactivity and bone marow production parameters.

In Fig. 9b and 9d we show that similar tendencies are found in the CA. Increasing σ increases the functional connectivity sligthly (Fig. 9b). In Fig. 9b the connectivity increases from 4 for $\sigma = 1$ (i.e., 13 neighbors) to 13 for $\sigma = 5$ (i.e., 385 neighbors). Similarly, the connectivity slightly increases with P_R, see Fig. 9d. The fact that the connectivity hardly depends on the neighborhood size is as counterintuitive as the fact that connectivity hardly depended on the matching probability in the bit-string model. The explanation for this counterintuitive phenomenon is similar for both systems. First, repertoire selection reduces the number of clones in the actual repertoire when clones have too many interactions. In the bit-string paper we discussed how this form of self-organization can be interpreted as a form of self-regulatory completeness (De Boer & Perelson, 1991). Second, because of the pattern formation, clones tend to be more similar which reduces the connectivity.

The error bars in Fig. 9b and 9d indicate the average standard deviation of the connectivity. (Each connectivity point is based upon ten samples, so each error bar is the average of ten standard deviations). The figure shows that the standard deviation increases with σ and P_R. This is another manifestation of the observation that the patterns become more ordered if either σ or P_R increases. Due to the pattern formation some areas are highly connected and some areas are lowly connected. Thus, the distribution of connectivities becomes more variable. Interestingly, in Fig. 9c of the bit-string model one can also see that the standard deviation of the connectivity increases with bone marrow production. This can now also be explained in terms of the increase in the order due to larger neighborhoods or the faster recuitment.

Fields

The histograms in Fig. 10 depict the distribution of field strengths for active B cells (Fig. 10a,b) and for unused sites in the shape space (Fig. 10c,d). The white bars denote the proportion of sites having a small field, i.e., $h(\mathbf{x}) \leq \exp[\theta_1]$, the gray bars denote stimulatory field strengths, i.e., $\exp[\theta_1] < h(\mathbf{x}) < \exp[\theta_2]$, and the striped bars denote suppressive fields, i.e., $h(\mathbf{x}) \geq \exp[\theta_2]$. Thus 45% of the used parts of shape space are stimulated (Fig. 10a,b) and 80% of the unused parts of shape space (Fig. 10c,d) are

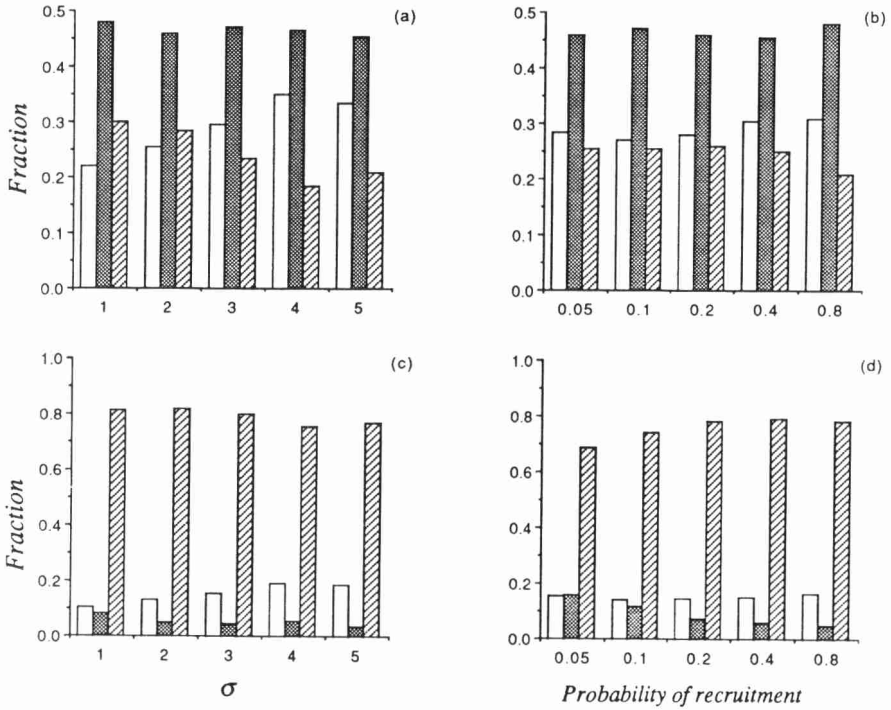

Figure 10. The distribution of field strengths of clones in the actual repertoire (a,b) and of the un-used sites (c,d). The white bars denote the proportion of sites having a small field, i.e., $h(\mathbf{x}) \leq \exp[\theta_1]$, the gray bars denote stimulatory field strengths, i.e., $\exp[\theta_1] < h(\mathbf{x}) < \exp[\theta_2]$, and the striped bars denote suppressive fields, i.e., $h(\mathbf{x}) \geq \exp[\theta_2]$.

suppressed. Both percentages hardly depend on σ or P_R. In the bit-string model we found that the majority of clones in the repertoire were suppressed. Here we find that only 20–30% of the actual repertoire is suppressed. An explanation for this discrepancy might be that suppressed clones are more quickly removed in the CA model than in the bit-string model. In the bit-string model we introduced more than one cell per recruitment event. Thus it takes longer to for the population to disappear by natural decay. Additionally, because in the bit-string model antibodies could be long-lived clones could persist for longer times.

There seems to be a slight effect of the neighborhood size on the ratio of suppressed and non-stimulated clones. Increasing σ increases the proportion of non-stimulated sites, and decreases the proportion of suppressed sites (Fig. 10c). This confirms earlier observations of other shape space models (De Boer *et al.*, 1992a).

Discussion

We have compared the behavior of an asynchronous CA model of the immune network with our previous ordinary diifferential equation/bit-string model. Our most important question was whether the inclusion of a realistic rate of the recruitment of new shapes would affect the results obtained with the bit-string model. Because all results seem to be similar this does not seem to be the case. Although we have been careful to point out how the two models can be derived from each other, it is important to realize how different the two approaches are. The fact that we find similar results for such a wide class of network models suggests that these results are generic.

Apart from the confirmation of our previous results in a more realistic parameter range, the CA model contributes to our understanding of the previous results on pattern formation. This is mainly due to the straightforward two dimensional representation of the CA. First, the 2D grayscale pictures of the CA really show that stimulatory areas become densily populated. This confirmed our interpretation of the same results in the bit-string model. Second, we have agrued that patterns become more ordered because recruitment may play the roles of annealing or randomness in voting rule systems (Toffoli & Margolus, 1988). A similar effect of random recruitment has also been demonstrated to increase the scale of spatial patterns of T and B cells in a CA model of T cell B cell segregation (Hogeweg, 1989). Similar effects may have played a role in the bit-string model and explain the observed deviation from a random distribution of Hamming distances (De Boer & Perelson, 1991).

The CA formalism makes it feasible to study high recruitment rates and very large networks. Thus, the more unrealistic formalism of a 2D CA shape space model has made it feasible to study the immune network for more realistic parameter regimes.

Acknowledgements

We thank Drs. Maarten Boerlijst for many helpful discussions. Portions of this work were performed under the auspices of the U.S. Department of Energy. It was supported in part by NIH Grant RR06555 (A.P.), and by the Santa Fe Institute through their Theoretical Immunology Program.

References

De Boer, R. J. (1988). Symmetric idiotypic networks: connectance and switching, stability, and suppression. In: Theoretical Immunology, Part Two. (A. S. Perelson, ed.). SFI Studies in the Science of Complexity., Vol. III. Addison-Wesley, Redwood City, CA, pp. 265–289.

De Boer R.J. (1991) Recent developments in idiotypic network theory. Neth. J. Med. 39: 254–262.

De Boer, R. J. & Hogeweg, P. (1989a). Memory but no suppression in low-dimensional symmetric idiotypic networks. Bull. Math. Biol. 51: 223–246.

De Boer, R. J. & Hogeweg, P. (1989b). Unreasonable implications of reasonable idiotypic network assumptions. Bull. Math. Biol. 51: 381–408.

De Boer, R. J., Kevrekidis, I. G. & Perelson, A. S. (1990). A simple idiotypic network model with complex dynamics. Chem. Eng. Sci. 45: 2375–2382.

De Boer, R. J. & Perelson, A. S. (1991). Size and connectivity as emergent properties of a developing immune network. J. Theor. Biol. 149: 381–424.

De Boer R. J., Segel L. A. & Perelson A. S. (1992a). Pattern formation in one and two dimensional shape space models of the immune system. J. Theor. Biol. **155**, 295–333.

De Boer R. J., Neumann A. U., Perelson A. S., Segel L. A. & Weisbuch, G. W. (1992b). Recent approaches to immune networks. In: Proceedings First European Biomathematics Conference, (Capassso, V. & Demongeot, P., eds.), Springer, Berlin (in press).

De Boer R. J., Kevrekidis I. G. & Perelson A.S. (1992c) Immune network behavior I: From stationary states to limit cycle oscillations. ~~(submitted).~~ Bull. Math. Biol 1993

De Boer R. J., Kevrekidis I. G. & Perelson A.S. (1992d) Immune network behavior II: From oscillations to chaos and stationary states. (submitted). Bull. Math. Biol 1993

De Boer R. J. & Van der Laan, J. D. (1992). A cellular automaton model of the immune network. In: Thinking about Biology, (Stein, W.D & Varela, F. J., eds.), Addison-Wesley, Redwood City, CA. 1993

Farmer, J. D., Packard, N. H. & Perelson, A. S. (1986). The immune system, adaptation, and machine learning. Physica D22: 187–204.

Farmer, J. D., Kauffman, S. A., Packard, N. H., & Perelson, A. S. (1987). Adaptive dynamic networks as models for the immune system and autocatalytic sets. Annals New York Acad. Sci. 504: 18–130.

Fish, S. Zenowich. E., Fleming, M. & Manser, T. (1989) Molecular analysis of original antigenic sin. I. Clonal selection, somatic mutation, and isotype switching during a memory B cell response. J. Exp. Med. 170: 1191–1209.

Freitas, A. A., Rocha, B. & Coutinho, A. (1986). Lymphocyte population kinetics in the mouse. J. Immunol. 91: 5–37.

Hogeweg, P. (1989) Local T–T and T–B interactions: a cellular automaton approach. Immunol. Letters 22: 113–122.

Holmberg, D., Andersson, Å., Carlson, L. & Forsgen, S. (1989). Establishment and functional implications of B-cell connectivity. Immunol. Rev. 110: 89–103.

Jerne, N. K. (1974). Towards a network theory of the immune system. Ann. Immunol. (Inst. Pasteur) 125 C: 373–389.

Klinman, N. R. (1972). The mechanism of antigenic stimulation of primary and secondary clonal precursor cells. J. Exp. Med. 136: 241–260.

Klinman, N. R., Press, J. L., Pickard, A. R., Woodland, R. T. & Dewey, A. F. (1974). Biography of the B cell. In: The Immune System, Genes, Receptors, Signals, Sercarz, E. E., Williamson, A. R. & Fox, C. F., eds. Academic Press, New York, pp. 357–365.

Murray, J. D. (1989). Mathematical Biology. Springer-Verlag, Berlin.

Neumann, A. U. & Weisbuch, G. (1992). Window automata analysis of population dynamics in the immune system. Bull. Math. Biol. 54: 21–44.

Neumann, A. U. & Weisbuch, G. (1992). Dynamics and topology of idiotypic networks. Bull. Math. Biol. ~~(in press)~~. 54: 699 - 726.

Perelson, A. S. (1984). Some mathematical models of receptor clustering by multivalent ligands. In: Cell Surface Dynamics: Concepts and Models (A. S. Perelson, DeLisi, C. & Wiegel, F. M., eds.), Marcel Dekker, New York, pp. 223–276.

Perelson, A. S. (1988), Toward a realistic model of the immune system. In: Theoretical Immunology, Part Two, SFI Studies in the Sciences of Complexity (A. S. Perelson, ed.), Addison-Wesley, Redwood City, CA, pp. 377-401.

Perelson, A. S. (1989). Immune network theory. Immunol. Rev. 110: 5–36.

Perelson, A. S. & Oster, G. F. (1979) Theoretical studies on clonal selection: minimal antibody repertoire size and reliability of self-non-self discrimination. J. Theor. Biol. 81: 645–670.

Perelson, A. S. & DeLisi, C. (1980). Receptor clustering on a cell surface. I. Theory of receptor cross–linking by ligands bearing two chemically identical functional groups. Math. Biosciences 48: 71–110.

Perelson, A. S. & Segel, L. A. (1991). On the shape-space approach to the immune system: A B cell antibody model. J. Stat. Phys. 63: 1113–1131.

Press, W. H., Flannery, B. P., Teukolsky, S. A. & Vetterling, W. T. (1988). Numerical Recipes in C. The Art of Scientific Computing., Cambridge University Press, Cambridge.

Riley, R. L. & Klinman, N. R. (1986). The affinity threshold for antigenic triggering differs for tolerance susceptible immature precursors vs mature primary B cells. J. Immunol. 136: 3147–3154.

Segel, L. A. & Perelson, A. S. (1988). Computations in shape-space: a new approach to immune network theory. In: Theoretical Immunology (A. S. Perelson, ed.), Part Two, SFI Studies in the Science of Complexity., Vol. III, Addison-Wesley, Redwood City, CA, pp. 321–343.

Segel, L. A. & Perelson, A. S. (1989). Shape-space analysis of immune networks. In: Cell to Cell Signalling: From Experiments to Theoretical Models, (A. Goldbeter, ed.), Academic Press, New York, pp. 273–283.

Stewart, J. & Varela, F. J. (1989). Exploring the meaning of connectivity in the immune network. Immunol. Rev. 110: 37–61.

Stewart, J. & Varela, F. J. (1990). Dynamics of a class of immune networks. II. Oscillatory activity of cellular and humoral components. J. Theor. Biol. 144: 103–115.

Stewart, J. & Varela, F. J. (1991). Morphogenesis in shape-space. Elementary metadynamics in a model of the immune network. J. Theor. Biol.153: 477–498.

Toffoli, T. & Margolus, N. (1987) Cellular Automata Machines. A New Environment for Modeling., MIT Press, Cambridge MA.

Varela, F. J., Coutinho, A., Dupire, B. & Vaz, N. N. (1988). Cognitive networks: immune, neural, and otherwise. In: Theoretical Immunology, Part Two, (A. S. Perelson, ed.), SFI Studies in the Science of Complexity., Vol. III, Addison-Wesley, Redwood City, CA, pp. 359–375.

Varela, F. J. & Stewart, J. (1990). Dynamics of a class of immune networks. I. Global stability of idiotype interactions. J. Theor. Biol. 144: 93–101.

Varela, F. J. & Coutinho, A. (1991). Second generation immune networks. Immunol. Today 12: 159–166.

Vichniac, G. (1986). Simulating physics with cellular automata. Physica 10D: 96–115.

Weisbuch, G. (1990). A shape space approach to the dynamics of the immune system. J. Theor Biol. 143: 507–522.

Weisbuch, G., De Boer, R. J. & Perelson, A. S. (1990). Localized memories in idiotypic networks. J. Theor. Biol. 146: 483–499.